

Fullerenes in the interstellar gas around IC 348 stars with protoplanetary disks

S. Iglesias-Groth^{1,2*}

¹ Instituto de Astrofísica de Canarias, La Laguna 38200, Spain

² Departamento de Astrofísica de la Universidad de La Laguna, Avda. Francisco Sánchez, La Laguna, 38200, Spain

2018

ABSTRACT

We present the detection of fullerenes C₆₀ and C₇₀ in the **interstellar gas nearby** stars hosting protoplanetary disks in the few Myr old IC 348 star-forming region of the Perseus Giant Molecular Cloud. Mid-IR vibrational transitions of C₆₀ and C₇₀ in emission are reported in *Spitzer* IRS spectra of the interstellar material near three IC 348 stars (LRLL 1, 2 and 58). The rather low C₆₀ and C₇₀ vibrational temperatures, 200–300 K, suggest that fullerenes are attached to dust grains in the material around these very young stars. Bands of the C₆₀⁺ and C₆₀⁻ are also **tentatively identified** in two of these stars from which we infer ionization fractions of 20 and 10 %, respectively. If the abundances derived from the observed emission lines were representative of the abundances in the protoplanetary disks around these stars we estimate that fullerene C₆₀, the most abundant of the two species, could host ~ 0.1 % of the total available carbon in the existing disks. This heavily relies on estimates of the intensity of the UV radiation field nearby these stars. The accretion of fullerenes in the early phases of planet formation may have implications on the chemistry of complex organic molecules in young forming planets. Accreted fullerenes may provide a reservoir of pentagonal and hexagonal carbon rings which could be important as building blocks of prebiotic molecules.

Key words: molecules – young stars - protoplanetary disks circumstellar medium

1 INTRODUCTION

Since the discovery of fullerenes C₆₀ and C₇₀ by Cami et al. (2010) in the young planetary nebula Tc1, using mid-IR spectra from *Spitzer Space Telescope*, these molecules were subsequently identified in reflection nebulae (Sellgren et al. 2010; Berne et al. 2013) several planetary (Garcia-Hernandez et al. 2011) and protoplanetary (Zhang & Kwok 2011) nebulae and in post-AGB stars (Gielen et al. 2011).

Fullerenes are efficiently formed in vaporization experiments of graphite (Kratschmer et al. 1990) and could also be formed in asymptotic giant branch stars (AGB) where circumstellar molecular synthesis is very rich. Fullerenes are rather stable molecules able to survive under the harsh conditions of the ISM as suggested by observations in several young stellar objects (Roberts et al. 2012) and by the ubiquitous presence of the diffuse interstellar bands at 957.7 and 963.2 nm which are associated to the cation C₆₀⁺ (Foing & Ehrenfreund 1994, 1997; Walker et al. 2015; Campbell et al. 2016). These authors have inferred that a significant fraction

of interstellar carbon is located in the C₆₀ cation, although original estimates of order 0.9% have been recently revised to values down to 0.1 % by Berne et al. (2017) who used the new oscillator strengths measured by Campbell et al. (2016). These cation bands were also detected in one protoplanetary nebula by Iglesias-Groth & Esposito (2013) who inferred that 0.86% of the carbon abundance in the nebula was in the form of the C₆₀ cation using the old oscillator strengths. Such abundances are consistent with fullerene concentration values of order 0.05–0.1 ppm which are similar to some controversial claims in meteorites (Becker & Bunch 1997; Becker et al. 1994), as debated by (Heymann 1997; Hammond & Zare 2008), and to the values inferred from the UV bump at 217.5 nm under the assumption that this prominent feature of extinction is caused by fullerenes (Iglesias-Groth 2004). At such abundances, fullerenes can play an important role in interstellar chemistry (Omori 2016).

The main driver for the formation of fullerenes is temperature see e.g. Jager et al. (2009). The presence of fullerenes in some planetary nebulae where bands of polycyclic aromatic hydrocarbons (PAHs) are absent appears also consistent with laboratory studies showing that the ef-

* E-mail: sigroth@iac.es

iciency of fullerene formation is favoured in hydrogen-poor environments (Cami et al. 2010). However, observations also show the coexistence of fullerenes and PAHs in planetary nebulae of the Magallanic clouds and other nebulae (Sellgren et al. 2010). It is therefore important to extend fullerene studies to other hydrogen rich astrophysical contexts. The circumstellar material near very young stars hosting protoplanetary disks is particularly interesting in this respect, as numerous spectroscopic studies in the near, mid/far infrared and millimeter range (see Henning & Semenov 2013) reveal a rich chemistry that may lead to the formation of a large variety of complex organic molecules in these disks. Among the various chemical ingredients detected in disks: silicates, H₂, CO, ices and organic molecules like PAHs are common and remarkably abundant. In the inner disk regions, Spitzer has detected a rich organic chemistry with species in the warm gas (T=200-1000 K) including CO, CO₂, C₂H₂, CN and HCN (Teske et al. 2011). It is important to establish the presence of fullerenes in protoplanetary disks and how they contribute to this organic chemistry. In this work, we report the detection of C₆₀ and C₇₀ in the circumstellar material near three stars hosting protoplanetary disks in the young star cluster IC 348 (age ~ 2 Myr, distance to the Sun 316 pc, Herbig et al. (1998) located next to the well known molecular complex of Perseus (Cernis et al. 1993; Snow 1994; Herbig et al. 1998; Luhman et al. 2003). Observations made with Spitzer show that half of the stars in this cluster have a circumstellar disk, of which 60% are gross or primordial disks.

2 OBSERVATIONS

2.1 The stars and the circumstellar material

We present results on the central star and most luminous member of IC 348 (LRLL 1, Luhman et al. 1998) and for another two stars with evolved disks LRLL 2 and LRLL 58 selected because of the availability of multiple observations by Flaherty et al. (2012). The stellar parameters are listed in Table 1. Spitzer maps reveal that the IR emission surface brightness peak of the Perseus cloud coincides with the location of LRLL 1 (HD 281159) a B5 V star. It is a binary star (separation 0.6 arcsec) with an extended disk structure mapped by Olofsson et al. (2012) using polarimetry. The polarimetric measurements reported by these authors and the ISO measurements at 16 μ m show a disk structure extending more than 20 arcsec in the SE-NW direction (with less emission in the NW part). This structure was first identified by Kalas et al. (1997) who proposed that it could be due to a protoplanetary disk. This hypothesis was questioned by Rebull et al. (2007), but the observations of Olofsson et al. (2012) suggest that the structure is indeed linked to circumstellar material near the star, which could be due to a protoplanetary disk or to the disruption of an accretion disk.

The star LRLL 2 is an A2-type with stable photospheric flux and near/mid IR excess consistent with an optically thick dust at T > 1000 K. LRLL 2 is a pre-main-sequence star with a bolometric luminosity of 137 L_⊙, a radius of 5 R_⊙ and a mass of ~ 3.5 M_⊙ based on the Siess et al. (2000) 3 Myr isochrones. Espaillat et al. (2012) find that the infrared SED can be fit with optically thick material that extends inward

to the dust destruction radius 1.7 AU. In Figure 8 of this paper the SED of LRLL2 is fitted with irradiated accretion disk models which incorporate dust settling (see their Table 2). According to the model, the inner wall dominates the emission in the NIR, the wall and disk both contribute to the MIR emission, and the disk dominates the emission at longer wavelengths. Flaherty et al. (2012) propose the existence of an evolved protoplanetary disk in LRLL 2 (see their Fig. 2). Evolved disks are believed to lie between fully optically thick disks and debris disks.

The third object, LRLL 58 is an M1.3 star (Siess et al. 2000). Details on its infrared variability and gas properties are provided by Flaherty et al. (2012). The nature of the disk in LRLL 58 is addressed by Flaherty et al. (2012) in significant detail. The star shows H α emission clearly indicative of an ongoing accretion process which will have associated UV excess emission.

2.2 Data

The Infrared spectra of the IC 348 targets reported here were obtained with the InfraRed Spectrograph (IRS) Houck et al. (2004) onboard the *Spitzer Space Telescope* Werner et al. (2004). Targets were selected by visual inspection of the CASSIS atlas of spectra Lebouteiller et al. (2011) which provides reduced and flux calibrated background subtracted data (see details at <http://cassis.sirtf.com/>) in the spectral region 17-20 μ m where the strongest C₆₀ vibrational bands are located.

I have carried out a systematic search of C₆₀ and C₇₀ in stars with protoplanetary disks in IC348 and present here first results on a selection of systems with available disk studies in the literature Olofsson et al. (2012); Flaherty et al. (2012). The spectra were obtained with the low resolution module-short wavelength (SL; 5-20 μ m) as part of the programs ID:40272, ID: 2 (PIs: Muzzeron, J. Houck) and for LRLL2 also with the high resolution short wavelength module (SH; 9.5-19.5 μ m) as part of the program ID:40247 (PI: Calvet). The data processing is described elsewhere (see <http://cassis.sirtf.com/>). Details of the observational parameters and AORs can be found in Table 1. The CASSIS extracted spectra performs the background subtraction using the Adopt (Advanced Optimal Extraction") method described in detail by Lebouteiller et al. (2010). The particularity of this method is that the background profile is estimated for each row independently. Adopt makes use of a polynomial background whose parameters are determined for each row solving a set of n linear equations via a multi-linear regression algorithm. Two procedures are used (subtraction by order and by nod) to correct for the background, both provide similar results for our targets. The column **integrated spectra at the position of the stars** finally adopted here show the contribution of the emission lines in the circumstellar material near the stars under study superposed to the stellar continuum. **Spatially extended emission lines are seen at scales beyond the spatial profile of each of the three stellar targets.** The spatial scale of the IRS (approximately 5 arcsec per pixel) does not allow to disentangle emission lines originating in the disk material from emission lines produced in the reflection nebulae surrounding the stars. As any decomposition procedure would lead to rather uncertain solutions, the spectrum **extracted**

Table 1. Parameters of protoplanetary disk host stars

Object	RA	Dec	Sp.T	T_{eff} (K)	M_* (M_\odot)	L_* (L_\odot)	R_* (R_\odot)	A_V	Age (Myr)	AORKey	dist. from star
LRLL 1	03:44:34.20	+32:09:46.3	B5V	15400 ^h	6.15 ^l	1660 ^j	...	3.1 ^g	0.4 ^l	25310464 ^a	0.04"
LRLL 2	03:44:35.36	+32:10:04.6	A2	8970	3.5 ⁱ	137 ^f	5 ^f	3.2 ^g	3 ^m	22847744 ⁿ	0.01"
LRLL 58	03:44:38.56	+32:08:00.7	M1.3	3800	0.7 ^e	0.72 ^g	2.1 ^f	3.4 ^g	3 ^m	22966016 ^b	0.18"
										22968320 ^b	0.03"
										22968064 ^b	0.12"
										16269056 ^c	0.14"
										22967808 ^b	2.08"
										22961664 ^b	2.13"
										22966272 ^b	0.35"
										22966528 ^b	0.43"

^a Program ID 50043 (K.Misselt). ^b Program ID 40372 (J. Muzerolle). ^c Program ID 2 (J. R. Houck). ^d Program ID 179 (N. Evans). ^e Siess et al., 2000. ^f Luhman et al., 2003. ^g Flaherty et al., 2012, ^h Merin et al. 2004, Kalas et al. 1997, ⁱ Siess et al. 2000, ^j Olofsson et al. 2012, ^k Preibisch & Zinnecker 2001, ^l Montesinos et al 2009, ^m Cohen et al.2004, ⁿ Program ID 40247 (N. Calvet).

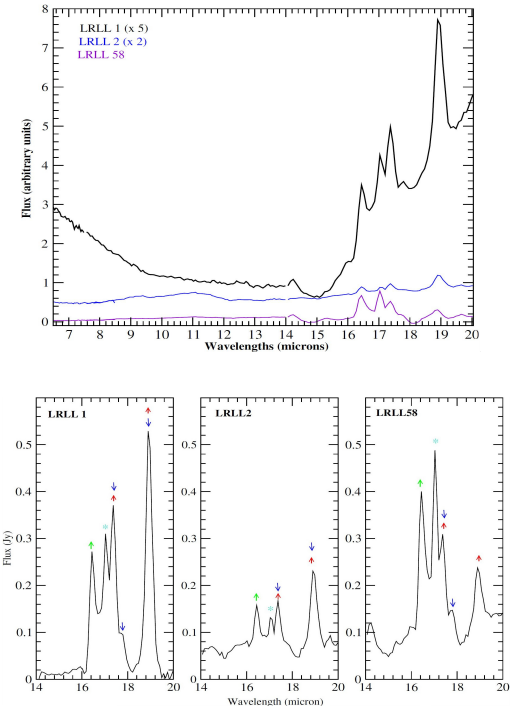


Figure 1. Top panel: Mid-infrared low resolution spectra of the stars LRLL 1, LRLL 2 and LRLL 58 (AORs: 253104464, 16269056 and 16755456, respectively). Fluxes in Jy have been arbitrarily scaled for clarity in the display. All spectra were obtained at distances less than 2" from each of the stars. Bottom panel: Continuum subtracted spectra of LRLL 1 (single spectrum), LRLL 2 (single spectrum) and LRLL 58 (average of 3 spectra obtained at distances less than 0.3 arcsec). Marks indicate the location of bands: C₆₀ (red), C₇₀ (blue), H₂ (asterisk) and PAH (green) bands. **The bands of C₆₀ and C₇₀ are blended.**

at the position of the star was adopted as the most appropriate description of the emission line spectrum in the material close to each star. For the low resolution data the orientation of the SL and LL slits are different, but the slits overlap on the target position and the extraction of the spectrum at this position minimize relative flux differences that may arise between the

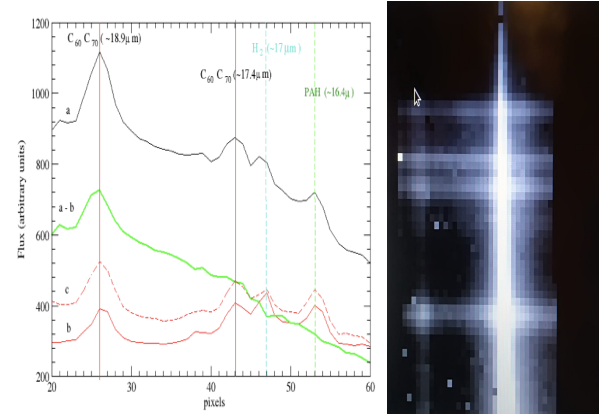


Figure 2. Right: Spectral 2-D image of LRLL1, the brightest star in the field. A second much fainter object is located at the left part of the image. Several emission lines are seen across the image. The strongest band at the bottom is the 18.9 μ m C₆₀ band. Left: Spectrum extracted at the position of LRLL 1, as an average of the two columns with the highest recorded signal in the image (label **a**, black line). For comparison, the average spectrum extracted from columns at the left of the star position (**b** red line), and to the right(**c** red dashed line). The subtraction of spectra **a-b** is also plotted (green line). Marks and solid vertical lines color codes: C₆₀ (red), H₂ (blue) and PAHs (green).

two observing modes due to a slightly different spatial location of the stellar profiles.

3 RESULTS AND DISCUSSION

Figure 1 (top panel) shows the Spitzer/IRS spectrum (7-20 μ m) for each of the targets. The distance of the slit position with respect to each star is indicated in Table 1. Note that in LRLL 1 the spectrum is dominated by a thermal dust continuum. A most prominent emission spectral band system is present in each star in the range 16-20 μ m which has a well resolved band at 18.9 μ m of C₆₀ (with potential contribution of C₇₀) and a mixture of PAHs at 16.4 μ m, H₂ (17 μ m) and fullerenes C₆₀ and C₇₀ at 17.4 μ m, see details in Fig. 1 (bottom panel) where the bands are marked and

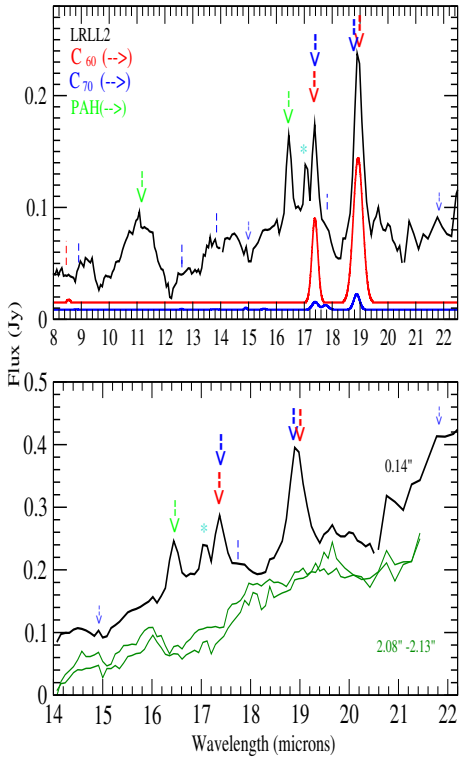


Figure 3. Spectra of the A2-type star LRLL 2. Bottom panel: spectrum obtained at a distance of 0.14" from the star (black line) in comparison with two spectra obtained at a distance of 2" (green line). Top panel: simulation of C_{60} and C_{70} mid-IR bands in comparison with the observed spectrum. Marks and solid lines color codes: C_{60} (red), C_{70} (blue) and PAHs (green).

the dust continuum was subtracted to LRLL 1. The relative strength of the fullerene and PAHs bands changes notably from the hottest B5 V star (LRLL 1, bottom-left panel) and the A2 V star (LRLL 2) where the fullerene bands are the dominant features, to the coolest star M1.3 (LRLL 58, bottom-right panel of Fig. 1), where the PAH band is dominant. The spatial behaviour of the emission bands in the circumstellar material close to each star varies notably. While the circumstellar bands are rather stable spatially in LRLL 2 and LRLL 58, in LRLL 1 inspection of the spatial evolution of the C_{60} band at 18.9 μm shows a stronger band closer to the location of the star. In Fig. 2 we plot the LRLL 1 spectrum extracted from various positions along the slit, the spectrum corresponding to the position of the star is labeled with a, we also plot average spectra extracted from nearby columns, left and right from the star location, labeled b,c, respectively. The difference spectrum a-b shows that at the position of the star the strength of the 18.9 μm is significantly higher than in more distant regions. This could be interpreted as evidence for a higher excitation of the C_{60} molecules because of the higher UV radiation field at the position of the star than in the nearby regions.

In Fig. 3 we present details of the bands and the continuum emission of the A2-type star LRLL 2. At the bottom panel we compare spectra where the bands of fullerenes and PAHs are clearly detected taken at the nominal position of the star (less than 0.14 arcsec) with spectra taken at separation of ~ 2 arcsec where these bands are not detectable. The

continuum emission remains similar at the two positions. In the upper panel of Fig. 3, the spectrum has been subtracted for the continuum emission. The positions of known bands of C_{60} (8.5, 17.4 and 18.9 μm) and C_{70} (17.4, 17.8, 18.9 and 21.8 μm) are marked. The 8.5 μm band is weak and blended with PAHs which makes difficult its assessment. Weak features of C_{70} appear to be present in the spectrum at 17.8 and 21.8 μm which is important in order to ascertain the relative contribution of this molecule to the strong bands at 17.4 and 18.9 μm . The solid red and blue lines in this panel represent computed simulations of the relative strengths of the bands of C_{60} and C_{70} which best fit the observed spectrum.

In Fig. 4 we plot IRS spectra of LRLL 2 obtained by Spitzer with the high spectral dispersion module ($R=600$). This is the only spectrum available at such dispersion for our stars. The panels of this figure display zooms of spectral regions where the position of known individual bands of C_{60} , C_{60}^+ and C_{70} are marked and the observed wavelength of the peak emission for each band is indicated. In addition to the bands at 18.9 and 17.4 μm mentioned above, the high resolution spectrum also shows evidence for bands at **12.63, 13.83, 14.90, 15.63 and 17.77 μm** . These bands can be attributed to C_{70} vibrational bands based on a comparison with published spectroscopic laboratory measurements. Iglesias-Groth et al. (2011) measured laboratory wavelengths and FWHMs for bands of C_{60} and C_{70} at different temperatures and found evidence for wavelength shifts of these bands depending on the temperature of the molecules and the adopted matrix. Table 2 lists for each band of C_{70} the range of wavelengths measured at different laboratory conditions. The table also lists wavelengths for the bands detected in the IRS high dispersion spectrum of LRLL 2 (typical measurement errors $\pm 0.01 \mu\text{m}$). Only bands in the range 10-20 μm covered by the IRS spectrum are given in the table. The agreement between laboratory wavelengths of C_{70} and observed wavelengths for the five cleanest potential bands of C_{70} is very good and provides strong support to the identification of C_{70} in LRLL 2. Other bands of C_{70} are also present in the spectrum, for instance, those measured at 17.4 μm and 18.7-18.9 μm but are likely blended with bands of C_{60} at very similar wavelengths. Complex broad features are detected in LRLL 2 at these wavelengths which could be contributed in principle by the two fullerene species. Interestingly, the wavelengths of the bands at 17.4 and 18.9 μm are the most sensitive to temperature and matrix conditions according to laboratory work. This makes more difficult to disentangle the contribution of each fullerene species to these features. The low resolution spectra of LRLL 2 also show broad features at 17.4 and 18.9 μm and very interestingly at 21.8 μm , the latter is consistent in wavelength with laboratory measurements of another rather clean band of C_{70} (Iglesias-Groth et al. 2011). The typical widths of individual, clean C_{70} bands measured in the high dispersion spectrum of LRLL2 are 0.02-0.03 μm which contrast with the ten times broader features observed at 17.4 and 18.9 μm , however these features receive contributions from C_{60} and C_{70} and possibly also from bands of the

ionized species, in particular C_{60}^+ is known to have a relatively strong band at $18.6\ \mu\text{m}$, these features are therefore intrinsically complex. In addition, as noted by Iglesias-Groth et al. (2011) in their laboratory work the widths of C_{60} bands are found to be very sensitive to the temperature and the matrix conditions. Particularly sensitive appears to be the $18.9\ \mu\text{m}$ band which, depending on the matrix and temperature conditions set at laboratory, displays a large range of widths spanning from $0.04\text{--}0.4\ \mu\text{m}$ and also wavelength shifts of up to $0.1\ \mu\text{m}$. The high dispersion spectrum of LRLL2 in the top right panel illustrates the rather complex structure of the $18.6\text{--}19.0\ \mu\text{m}$ feature, the weaker $17.4\ \mu\text{m}$ feature is also complex.

In the high dispersion spectrum of LRLL 2 displayed in Fig. 4 there are also features at 10.47 , 13.22 and $18.58\ \mu\text{m}$ which are fully consistent with wavelengths computed for the IR-active bands of C_{60}^+ by Berne et al. (2013) and therefore could be attributed to this cation. The bands at 10.47 and 18.58 are the strongest predicted for the spectral range covered by our observations with intensities 2–3 times higher than the 13.22 band (see Table 2 in the previous paper) and in fact, this intensity behaviour is observed in the spectrum. The other predicted lines are too weak and cannot be detected. These three bands are the only ones which could be detected in the high dispersion spectrum of LRLL 2. However in the low resolution spectrum it is possible to find features at 6.4 and $7.2\ \mu\text{m}$ which according to predictions are the strongest of the IR active modes of the C_{60}^+ . In summary, the detection of C_{60}^+ in LRLL 2 is claimed based on identification of the five strongest IR active bands.

In Table 3 we provide wavelengths, fluxes and full width half maximum (FWHM) measurements for the relevant fullerene C_{60} and C_{70} bands in the $7\text{--}22\ \mu\text{m}$ regions. In Table 4 we provide measurements for the bands (6.4 , 7.2 , 10.5 , 13.2 and $18.6\ \mu\text{m}$) of the C_{60}^+ in the stars LRLL 2 and 58. All measurements have been performed using the SPLIT routine of IRAF and its de-blending option was used wherever it was required to disentangle multiple components, particularly in the region $16\text{--}18\ \mu\text{m}$. Gaussian profiles were assumed for all the fits. The C_{60} features in the range $17\text{--}19\ \mu\text{m}$ have a typical width of $0.3\text{--}0.4\ \mu\text{m}$, wider than the spectral resolution of the instrument and similar to the widths observed in planetary nebulae (like Tc 1). The total flux of the feature at $18.9\ \mu\text{m}$ is rather stable among the observed circumstellar material ranging from 3×10^{-16} to $1 \times 10^{-15}\ \text{W m}^{-2}$, in spite of the very different luminosity and temperature of the studied host stars. The contribution of C_{70} to the total emission of the bands observed at $18.9\ \mu\text{m}$ and $17.4\ \mu\text{m}$ has been established using the information provided by other bands of this molecule assuming a simple model to describe band ratios, we find C_{70} contributions in the range 10–30% of the total band strengths.

Regions of the spectrum of LRLL 58 are plotted at the bottom right panel of Fig. 1 and in Fig. 5 where they are distributed in three panels for the sake of clarity. In each spectral range we mark the location of bands from PAHs and fullerenes C_{60} (neutral and cation) and C_{70} . Interestingly,

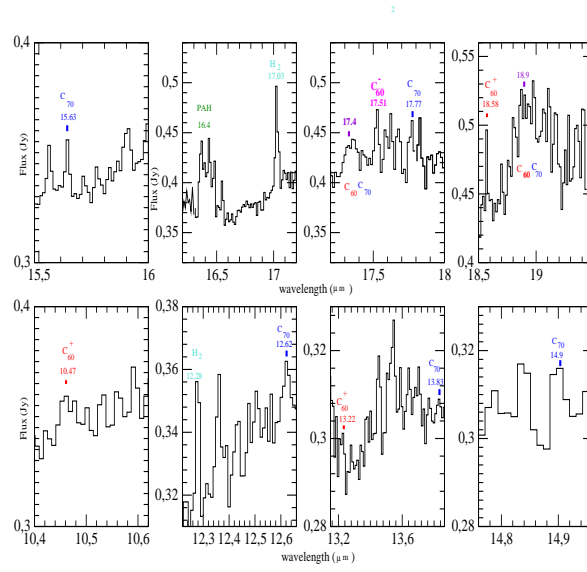


Figure 4. Spitzer mid-infrared HR spectra of the star LRLL 2 (AOR: 22847744).

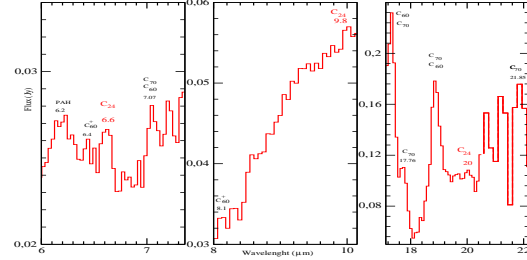


Figure 5. Mid-IR spectrum of LRLL 58 Marks and color codes: fullerene C_{60}^+ cation (6.4 , $8.1\ \mu\text{m}$), C_{70} (17.76 , $21.85\ \mu\text{m}$), C_{60} + C_{70} blends (7.1 , 17.4 , $18.9\ \mu\text{m}$), graphene C_{24} (red colour 6.6 , 9.8 , $20\ \mu\text{m}$)

the $16.4\mu\text{m}$ PAH emission in LRLL 58 is significantly enhanced with respect the $18.9\ \mu\text{m}$ C_{60} band (Fig. 1), contrary to what is observed in the other two targets of the sample where this PAH band appears weaker relative to fullerene emission. The relative enhancement of the PAH emission in this cooler object could be the result of a higher sensitivity of the PAH abundance to the physical conditions of the stellar radiation field. LRLL 58 has the lowest luminosity and the coolest effective temperature of the stars in our sample and this may favor the survival of PAHs. Fullerenes are expected to be more robust against radiation than PAHs. In the left and central panel of Fig. 5, the position of known bands of graphene C_{24} at 6.6 , 9.8 and $20\ \mu\text{m}$ predicted by Kuzmin & Duley (2011) are marked. We see features at these positions with fluxes at 3×10^{-17} , 1×10^{-17} and $0.6 \times 10^{-17}\ \text{W m}^{-2}$, respectively. This can be taken only as tentative evidence for graphene. Bands of the C_{60} cation are also marked in the spectrum of Fig. 5 with their fluxes reported in Table 3. While these are also weak bands, they appear consistent with high resolution observations of similar features in LRLL 2.

Table 2. Laboratory wavelengths of C_{70} bands and observed bands in the high dispersion spectrum of LRLL 2

Laboratory measurements (μm)	LRLL 2 obs. spectrum (μm)
12.61-12.62	12.62
13.80-13.81	13.83
14.90-14.91	14.90
15.64-15.67	15.63
17.62-18.07	17.77

Table 3. Measurements of fullerene bands in protoplanetary disks. Wavelength (μm) and Flux (Wm^{-2}). From low resolution (stars LRLL1 and LRLL58) and high resolution (star LRLL2)

Band	λ	LRLL 1 Flux	FWHM	λ	LRLL 2 Flux	FWHM	λ	LRLL 58 Flux	FWHM
21.8 μm band									
C_{70}	21.78	$\leq 5 \times 10^{-17}$					21.85	4.5×10^{-17}	
18.9 μm band									
Total	18.93	1.1×10^{-15}	0.33	18.93	2.7×10^{-16}	0.3	18.87	4.0×10^{-16}	0.35
C_{60}		9.8×10^{-16}			1.8×10^{-16}			1.8×10^{-16}	
C_{70}		8.0×10^{-17}			7.3×10^{-17}			1.5×10^{-16}	
17.4 μm band									
Total	17.36	9.8×10^{-16}	0.3	17.39	3.5×10^{-17}	0.3	17.36	8.6×10^{-17}	0.3
C_{60}		9.0×10^{-16}			2.8×10^{-17}			6.9×10^{-17}	
C_{70}		7.4×10^{-17}			7.0×10^{-18}			1.7×10^{-17}	
17.76 μm band									
C_{70}	17.76	9.6×10^{-17}	≤ 0.3	17.77	1.7×10^{-17}	< 0.2	~ 17.76	1.2×10^{-17}	≤ 0.3
15.6 μm band									
C_{70}					15.64	7.1×10^{-18}		15.56	2.8×10^{-17}
14.9 μm band									
C_{70}	14.95	7.5×10^{-18}		14.90	7.4×10^{-18}	$\gtrsim 0.05$	~ 14.94	1.4×10^{-17}	
12.6 μm band									
C_{70}					12.62	1.1×10^{-17}			
7.0 μm band									
$C_{60} + C_{70}$	7.1	1.5×10^{-17}		7.04	1.9×10^{-17}		7.07	2.0×10^{-17}	

3.1 Abundances

As discussed e.g. by Bernard-Salas et al. (2012) the excitation of circumstellar fullerenes may be understood mainly via thermal models or IR fluorescence models. The latter predict nearly constant $F(17.4 \mu\text{m})/F(18.9 \mu\text{m})$ ratios in a broad range of excitation energies and also fairly strong bands at 7 and 8.5 μm . Thermal models where the emitted power in each of the fullerene bands is proportional to the corresponding excited vibrational state can naturally explain observed flux ratios $F(17.4 \mu\text{m})/F(18.9 \mu\text{m})$ in the range 0.5-0.6 and the ~ 50 times weaker fluxes of the 7 and 8.5 μm bands w.r.t. the 18.9 μm band in our spectra (see the diagnostic diagram of Fig.5 in Bernard-Salas et al. (2012)).

From the fluxes in Table 2, it is possible to infer abundances of the fullerenes C_{60} and C_{70} by using thermal models and adopting the temperature dependence of the absorptivity for each fullerene transition Iglesias-Groth et al. (2011). This approach has been followed for instance by Garcia-Hernandez et al. (2011) in their study of fullerene abundances in planetary nebulae. I assume errors of 10 % in the flux determinations of C_{60} and of order 20 % for the weaker lines of C_{70} . In the case of LRLL 2, where both the low and high spectral resolution data are available, a good number of C_{70} bands are detected (12.6, 14.9 and 15.6 μm) which are essentially uncontaminated in the high dispersion spectrum. These bands are the basis for an initial thermal model solution for this molecule. Then, an iterative process is followed to obtain an estimation of the C_{70} fluxes at 18.9, 17.4 and 7.0 μm from a best-fit solution providing both the tempera-

ture of the emitting region ($T \sim 200 \text{ K}$) and the total number of emitting molecules, which is found at $N(C_{70}) = 1.5 \times 10^{44}$. The fit also provides an estimate of the fluxes for each of the three blended bands. The values are listed in Table 2 where total fluxes measured for these bands and the best estimate of the C_{70} and C_{60} contributions to the total fluxes are given. As a result only 30 % of the flux at 18.9 μm is contributed by C_{70} . The resulting thermal model for C_{60} band fluxes gives $N(C_{60}) = 3.2 \times 10^{44}$, a factor 2 more abundant than C_{70} and equilibrium temperature of 250 K. In addition, the five measured bands of C_{60}^+ (fluxes listed in Table 3) albeit weak and close to the sensitivity limit of the spectra, also provide a reliable model solution, resulting in $N(C_{60}^+) = 2.6 \times 10^{43}$. According to the thermal model, this implies that about 10 % of the C_{60} would be in the cation form.

The upper limits on the fluxes of the 7 and 8.5 μm bands limit our capacity to determine accurate equilibrium temperatures and abundances in the other two stars, but in the case of LRLL 58 where at least three bands of each neutral fullerene type are also detected in low resolution spectra, the preferred model solutions lead to $N(C_{60}) = 1 \times 10^{45}$ with a vibrational temperature of $T = 150 \text{ K}$ and $N(C_{70}) = 1 \times 10^{45}$ with vibrational temperature of 300 K. Very similar abundances of both species. It was also possible to measure some weak bands of C_{60}^+ in this star (see Table 3) from which it is inferred $N(C_{60}^+) = 2 \times 10^{42}$ and $T = 350 \text{ K}$. Indicating a much lower ionization fraction than in the previous star.

For LRLL 1 where only upper limits can be imposed to the flux of the 7 μm band, for C_{60} it is found equilibrium temperatures below 250 K and abundance values of 4×10^{46}

Table 4. Cation C_{60}^+ bands in LRLL 2 and LRLL 58: measured wavelengths (μm) and fluxes ($W m^{-2}$).

LRLL 2		LRLL 58	
λ	Flux	λ	Flux
6.45	0.5×10^{-17}	6.45	5.3×10^{-18}
7.22	1.2×10^{-18}	7.22	1.4×10^{-17}
10.47	2.2×10^{-17}		
13.22	6.8×10^{-18}	13.23	3.4×10^{-18}
18.56	1.4×10^{-17}		
		8.13	1.4×10^{-17}

with uncertainties of order 50 %. This star, which is the most luminous of the three under study, is by far the one with the strongest bands and the highest value of $N(C_{60})$ according to these models.

An alternative way to estimate fullerene abundances in our sources is via the assumption that all the UV energy absorbed by fullerenes is released in the IR, which would be correct if there were no other relaxation channels. This is valid for C_{60} internal energies (see Berne et al. (2017)). If we also assume that the UV absorption cross section of the neutral and the cation are similar, we can obtain a quick estimate of the ionization fraction by adding the fluxes measured for IR bands of these species in our targets. In the case of LRLL2 the total flux measured in bands of C_{60}^+ is $5 \times 10^{-17} W m^{-2}$ and for neutral C_{60} is 2.3×10^{-16} , therefore the ionization fraction of C_{60} is 21%, higher than the value given above from thermal models. In Fig. 4 we also show the detection of a clear band at $17.51 \mu m$ with a flux of $1.8 \times 10^{-17} W m^{-2}$ which we attribute to the anion C_{60}^- . In the low resolution spectrum of this star there is also a feature at $7.3 \mu m$ with flux $3 \times 10^{-17} W m^{-2}$ which can also be due to the anion. These two bands are the strongest vibronic bands known of the anion Kupser et al. (2008). Taking the sum of the fluxes emitted in these bands as an estimate of the total emitted IR flux by the cation, we infer the ionization fraction of 21 %, which should be strictly taken as a lower limit.

Following e.g. Berne et al. (2017), the total IR intensity ($W m^{-2} sr^{-1}$) emitted by C_{60} molecules is $I_{tot} = n(C_{60}) \times \sigma_{UV} \times G_0 \times 1.2 \times 10^{-7}$ where $n(C_{60})$ is the column density of C_{60} , $\sigma_{UV} = 4.2 \times 10^{-16} cm^2$, G_0 is the radiation field. For the Perseus molecular complex is generally adopted a value of $G_0=1$, see e.g. the low spatial resolution studies of AME (Anomalous Microwave Emission) in Perseus Gnova-Santos et al. (2015). However as shown in the study by ? large variations in the far UV (FUV) radiation field can exist in the Perseus star-forming region IC 348 where the stars of this work are located. In Table 3 of the later paper the variations of the intensity of the FUV radiation field are quantified using different approaches. Depending on the adopted method, the center of the cluster where star LRLL 1 (HD 211958) is located has a factor 10-80 higher intensity field than the less intense regions of the star-forming region which are comparable to the general interstellar field. I will adopt here an intermediate value of $G_0=45$ for the radiation field in the vicinity of LRLL 1 and $G_0=20$ for stars LRLL 2 and 58.

The total fluxes of C_{60} IR bands obtained from Table 3 are divided by the area subtended (in sr) by the spatial extension of each extracted spectrum in order to provide a determination of I_{tot} . The values obtained for LRLL 1,

LRLL2 and LRLL 58 are 4×10^{-7} , 2×10^{-7} and $0.5 \times 10^{-7} W m^{-2} sr^{-1}$, respectively, giving C_{60} column densities of 2, 1 and $0.5 \times 10^{14} cm^{-2}$ for each target. Using the expression $f_C^{C_{60}} = n(C_{60}) \times 60 / (N(H) \times [C])$ where [C] is the carbon to hydrogen ratio adopted as 1.6×10^{-4} Sofia et al. (2004), and taking $N(H) = 4.8 \times 10^{22}$ from Sun et al. (2008) for the central part of the IC 348 cluster, it yields abundances of the gas phase carbon locked on C_{60} of 1.6×10^{-3} , 0.8×10^{-3} and 0.4×10^{-3} , for stars LRLL 1, 2 and 58, respectively. These values of 0.16-0.04 % compare well with previously reported values in star-forming regions (Castellanos et al. 2014; Berne et al. 2017). This value is of order of those found in planetary nebulae (Garcia-Hernandez et al. 2011) suggesting that a significant fraction of fullerenes formed in proto and planetary nebulae can survive the harsh conditions of the interstellar medium and become incorporated into the circumstellar material of young star-forming regions like IC 348.

The typical total disk masses in IC 348 stars as measured from millimeter fluxes (Lee et al. 2011) are in the range 0.002 - $0.006 M_\odot$. Assuming for the disks of our stars a typical mass of $0.004 M_\odot$ and solar metallicity, we can estimate the total mass of carbon in the disks to be of order $6.2 \times 10^{-7} M_\odot$. Applying the derived percentage of carbon locked in fullerenes, we estimate that the disks in our stars contain between 8 and $2 \times 10^{-9} M_\odot$ in the form of C_{60} , corresponding to a number of C_{60} molecules in the range 10^{46} - 10^{45} . This suggests that a large fraction of the $N(C_{60})$ obtained with the thermal models is actually residing in the protoplanetary disks hosted by these stars.

4 CONCLUSIONS

We present the detection and the determination of fullerene abundances in circumstellar matter of the star-forming region IC 348 using the CASSIS atlas of spectra from the *Spitzer Space Telescope*. Detection of bands of C_{60} at 7.04 , 17.4 and $18.9 \mu m$ in low resolution spectra and bands of C_{70} at 12.6 , 13.8 , 14.9 , 15.6 , 17.8 , 18.9 and $21.8 \mu m$ in high and low resolution spectra are reported. The bands of PAHs ($16.4 \mu m$) and H_2 ($17 \mu m$) coexist with fullerene bands in the spectra of the three targets under study. Contrary to PAHs, fullerenes appear to be little sensitive to the physical conditions of the circumstellar material. The derived vibrational fullerene temperatures are below 300 K which indicates that the emitting molecules are likely attached to dust grains. We also detect several bands **which could be due** to the ionized species C_{60}^+ (10.47 , 13.22 and $18.58 \mu m$) and C_{60}^- (7.3 and $17.51 \mu m$) from which we infer ionization fractions of 20 and 10 %, respectively for the best mea-

sured spectrum. Fullerenes could be incorporated into planets during their early stages of formation in protoplanetary disks. If the derived percentage of gas-phase carbon locked in fullerenes were representative of the material conforming the protoplanetary disks in these stars, a large reservoir of fullerenes shall exist in disks. Fullerenes consist of pentagonal and hexagonal carbon structures that may supply in young planetary environments building blocks for the formation of complex organic molecules (Iglesias-Groth et al. 2013) like amino acids and DNA bases for which carbon ring structures are an essential part.

ACKNOWLEDGEMENTS

Based on observations made with the *Spitzer* mission. I thank CASSIS for access to the spectroscopic database. The MINECO project ESP2015-69020-C2-1-R for financial support and Rafael Rebolo for a critical reading of the manuscript and valuable suggestions and comments on its contents.

REFERENCES

- Becker, L. & Bunch, T.E. 1997, Meteoritics & Planetary Science 32, 479
- Becker, L., Bada, J.L., Winans, R. E. & Bunch, T.E. 1994, Nature, 372, 507
- Bernard-Salas, J., Cami, E. et al. 2012, ApJ 757, 41
- Berné, O., Mulas, G. & Joblin, C., 2013, A&A 550, L4
- Berné, O., Cox, N. L. J., Mulas, G. & Joblin, C., 2017, A&A 605, L1
- Cami, J., Bernard-Salas, J., Peeters, E., & Malek, S. E. 2010, Science 329, 1180
- Campbell, E. K., Holz, M. & Maier, J. P. 2016, ApJ826, L4
- Castellanos, P., Berné, O., Sheffer, Y., Wolfire, M. G., & Tielens, A. G. G. M. 2014, ApJ, 794, 83
- Cernis, 1993, BaltA, 2, 214
- Cieza, L. & Baliber, N. 2006, ApJ, 649, 862
- Espaillat, C., Ingleby, L., Hernandez, J., et al. 2012, ApJ737, 103
- Flaherty K. M., Muzerolle J., Rieke G., Gutermuth R., Balog Z., Herbst, W., Megeath, S. T. & Kun, M. 2012, ApJ748, 71
- Foing, B. H. & Ehrenfreund, P. 1994, Nature 369, 296
- Foing, B. H. & Ehrenfreund, P. 1997, A&A 317, L59
- Garcia-Hernández, A.D. Iglesias-Groth, S., et al. 2011, ApJ737, L30
- Genova-Santos, R., Rubino-Martin, J.A., Rebolo R. et al. 2015, MNRAS, 452, 4169
- Gielen, C., Cami, J., Bouwman, J., Peeters, E. & Min, 2011, A&A 536, A54
- Kupser, P., Steill, J. D., Oomens, J., Meijer, G., & von Helden, G. 2008, Phys.Chem. Chem. Phys., 10, 6862
- Hammond, M.R., Zare, R. N., 2008, GeCoA, 72, 22, 5521
- Herbig, G. H. 1998, ApJ, 497, 736
- Henning, T. & Semenov, D. 2013, ChRv., 113.9016
- Heymann, D. 1997, ApJ489, L111
- Houck, J. R et al. 2004, AAS 204, 3304
- Iglesias-Groth 2004, ApJ608, 37
- Iglesias-Groth, S., Cataldo, F., & Manchado, A. 2011, MNRAS, 413, 213
- Iglesias-Groth, S. & Esposito, M. 2013, ApJ776, L21
- Iglesias-Groth, S., Hafez, Y., Angelini, G. & Cataldo, F. 2013, J. Rad. Nuc. Chem., 298, 1073-1083
- Jager C. et al. 2009, ApJ, 696, 796
- Kalas, P. & Jewitt, D. 1997, Nature 386, 52
- Krätschmer, W., Lamb, L. D., Fostiropoulos, K., & Huffman, D. R. 1990, Nature 347, 354
- Kupser, P., Steill, J. D., Oomens, J., Meijer, G., & von Helden, G. 2008, Phys. Chem. Chem. Phys., 10, 6862
- Kuzmin, S. & Duley, W.W 2012, arXiv:1103.2989
- Lebouteiller, V., Barry, D.J., Spoon H. W. W., Bernard-Salas, J., Sloan G. C. & Houck, J. R. 2011, ApJS196, 8
- Lebouteiller, V., Bernard-Salas, J., Sloan G. C & Barry, D.J., 2010, PASP122, 231
- Lee N., Williams, J.P. & Cieza, L. 2011, 736, 135
- Luhman, K. L., Rieke, G.H., Lada C.J. & Lada E.A. 1998 ApJ508, 347
- Luhman, K. L., et al. 2003, ApJ, 593, 1093
- Merín, B., Montesinos, B. & Eiroa, C. 2004, A&A, 419, 301
- Montesinos, B.; Eiroa, C., Mora, A.; Mern, B. 2009, A&A, 495, 901
- Omont, A. 2016, A&A 590, A52
- Olofsson, G., Nilsson, R., Florén, H-G, Djupvik, A. & Aberasturi, M.. 2012, A&A, 544, 43
- Preibisch, T., Stanke, T & Zinnecker, H. 2001, ASPC, 223, 1556
- Rebull, L.M., Stapelfeldt, K.R., Evans, N.J.H. et al. 2007, ApJS171, 447
- Roberts, K.R.G., Smith, K.T. & Sarre, P.J. 2012, MNRAS, 421, 3277-3285
- Sellgren, K. et al. 2010, ApJ, 722, L54
- Siess, L. Dufour, E. & Forestini, M., 2000, A&A 358, 593
- Snow, T. P., 2004, ASPC, 309, 93
- Sofia, U.J., Lauroesch, J.T., Meyer, D. M., Cartledge, S.I.B., 2004, ApJ, 605, 272
- Sun, K., Ossenkopf, V., Kramer, C., Mookerjea, B., Rllig, B., Cubick, M. & Stutzki J., 2008, ApJ, 489, 207
- Teske et al. 2011, Astrophys. J., 734, 27
- Walker, G. A. H., Campbell, E. K. Maier, J. P. & Bohlende, D. 2015, ApJ, 843, 56
- Werner, M. W. et al. 2004, ApJS, 154, 1
- Zhang, Y & Kwok, S. 2011, ApJ, 730, 126